Electrochemically Controlled Ion Dynamics in Porphyrin Nanostructures

Andrés F. Molina-Osorio,[†] José A. Manzanares,[‡] Alonso Gamero-Quijano[†] and Micheál D Scanlon*[,†,§]

† The Bernal Institute and Department of Chemical Sciences, School of Natural Sciences, University of Limerick (UL), Limerick V94 T9PX, Ireland.

‡ Department of Thermodynamics, Faculty of Physics, University of Valencia, c/Dr. Moliner, 50, E-46100 Burjasot, Spain.

§ Advanced Materials and Bioengineering (AMBER) Centre, Ireland.

Corresponding authors:

*E-mail: micheal.scanlon@ul.ie

Abstract

The dynamics of ion intercalation into solid matrices influences the performance of key components in most energy storage devices (Li-ion batteries, supercapacitors, fuel cells, etc.). Electrochemical methods provide key information on the thermodynamics and kinetics of these ion transfer processes but are restricted to matrices supported on electronically conductive substrates. In this article, the electrified liquid|liquid interface is introduced as an ideal platform to probe the thermodynamics and kinetics of reversible ion intercalation with non-electronically active matrices. Zinc(II) meso-tetrakis(4-carboxyphenyl)porphyrins were self-assembled into floating films of ordered nanostructures at the water|α,α,α-trifluorotoluene interface. Electrochemically polarising the aqueous phase negatively with respect to the organic phase lead to organic ammonium cations intercalating into the zinc porphyrin nanostructures by binding to anionic carboxyl sites and displacing protons through ion exchange at neutral carboxyl sites. The cyclic voltammograms suggested a positive cooperativity mechanism for ion intercalation linked with structural rearrangements of the porphyrins within the nanostructures, and were modelled using a Frumkin isotherm. The model also provided a robust understanding of the dependence of the voltammetry on the pH and organic electrolyte concentration. Kinetic analysis was performed using potential step chronoamperometry, with the current transients composed of "adsorption" and nucleation components. The latter were associated with domains within the nanostructures where, due to structural rearrangements, ion binding and exchange took place faster. This work opens

opportunities to study the thermodynamics and kinetics of purely ionic ion intercalation reactions (not induced by redox reactions) in floating solid matrices using any desired electrochemical method.

Introduction

Charge transfer reactions at electrified interfaces critically influence the performance of devices with energy-related applications.[1,2] The continuous development of sustainable technologies relies on precise analysis of the thermodynamics and kinetics underlying the charge transfer reactions involved.[3] Of the different charge transfer phenomena, a molecular scale understanding of electron transfer across solid-liquid interfaces is now accessible.[4] However, such in-depth analysis remains a challenge for interfacial ion transfer between two different phases.

Ion transfer reactions are of major importance in many energy storage technologies. A key step during cycling of lithium-ion (Li-ion) batteries is the reversible ion transfer, termed intercalation and de-intercalation, of Li^+ between the electrolyte and cathode material.[4] For supercapacitor applications, conducting polymers exhibit pseudocapacitance through doping and de-doping of the polymer backbone, which involves intercalation and de-intercalation of electrolyte ions within the polymer film to maintain charge neutrality.[5] Ion exchange membranes (IEMs) are used in combination with electrochemical potential gradients to drive intercalation and de-intercalation, typically through an ion exchange mechanism, for the selective transport of certain ionic components between phases with different chemical compositions.[6,7] Such IEMs are critical to the operation of fuel cells,[8] electrolysers,[9] redox flow batteries,[10] reverse electrodialysers,[11] and microbial fuel cells.[12]

Electrochemical methods are particularly well suited to provide key information on the thermodynamics and kinetics of these ion transfer processes. However, their use is restricted to matrices supported on electronically conductive substrates, as is the case for Li-ion battery cathodes[13–15] or conducting polymer films,[16,17] where reversible ion transfer is coupled with a redox reaction. Analysis of ion transfer reactions in non-electronically conductive solids, such as IEMs, is more difficult to study, given that ion transfer proceeds through an ion exchange mechanism without a flow of electrons.[18,19] In this sense, the interface between two immiscible electrolyte solutions (ITIES),[20,21] such as that formed between water and suitable hydrophobic

organic solvents, offers an ideal platform to study the thermodynamics and kinetics of ion transfer reactions involving non-electronically conductive solids.

In the absence of redox-active species, polarisation of the ITIES induces the movement of aqueous and organic electrolyte ions to, and across, the liquid|liquid interface.[22,23] Thus, a film of solid materials floating at the interface will experience a markedly different ionic environment and interfacial aqueous pH depending on the applied interfacial Galvani potential difference ($\Delta_o^w\phi$ / V). In this article, we demonstrate that interaction of charged or easily ionisable functional groups within the floating solid materials with the aqueous and organic electrolyte ions gives rise to capacitive currents associated with purely ionic reactions. Previous studies involving functionalisation of the ITIES with non-conductive inorganic materials, such as zeolites[24–26] or silica,[27–31] were primarily motivated to develop sensor technology through charge- or size-selective ion transfer across the interface. Dryfe and co-works have reported electrochemically driven ion exchange involving zeolites floating at an ITIES, but no in-depth thermodynamic or kinetic analysis was performed.[32–34]

Herein, we study the thermodynamics and kinetics of electrochemically reversible ion intercalation at a floating film of self-assembled zinc(II) 5,10,15,20-(tetra-4-carboxyphenyl)porphyrin interfacial nanostructures (ZnPor-INs). The floating film effectively acts as an ion penetrable third phase separating the aqueous and organic phases. Cyclic voltammetry in the presence of the ZnPor-IN film was amenable to thermodynamic analysis using the Frumkin isotherm[13–15] and kinetic analysis was performed using potential step chronoamperometry.[35] These *purely ionic* voltammetric and current transient responses were analogous to those commonly associated with reversible ion intercalation coupled with electron transfer, as described for Li-ion battery cathodes and conducting polymer films. The distinctive shape of the cyclic voltammograms also indicated an electrochemically driven rearrangement of the porphyrin nanostructure at the liquid|liquid interface. These observations, connected with the presence of easily ionisable carboxyl groups within the ZnPor-IN film, were rationalised in terms of electrochemically-driven binding of organic cations at anionic carboxyl ($–COO^–$) groups and ion exchange of organic cations at neutral carboxyl (–COOH) groups in which protons are displaced. This concept is schematically shown in Schemes 1 and S1 (Supporting Information).

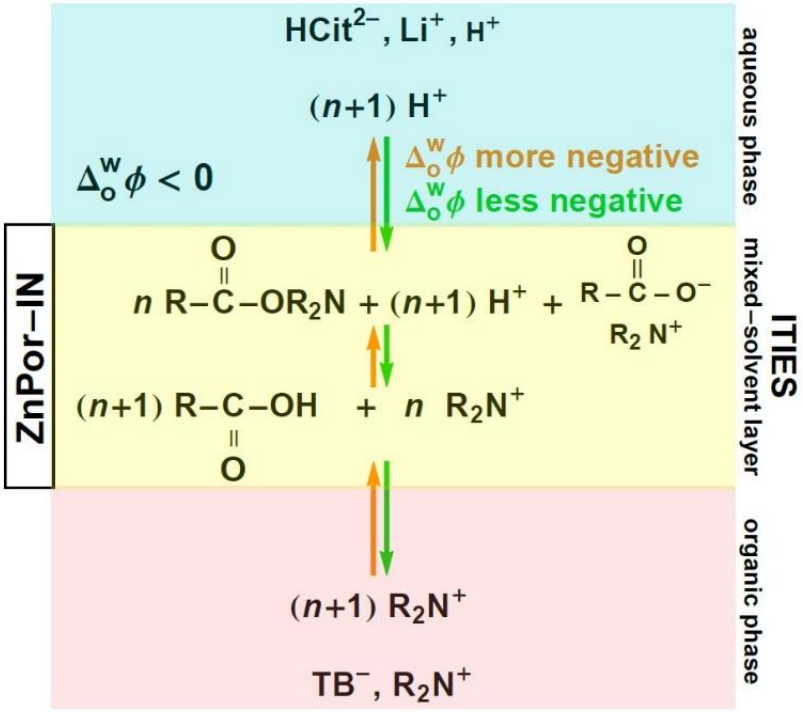

Scheme 1. Electrochemically-driven shifts in the chemical equilibria involving carboxyl groups in the ZnPor-IN film, aqueous protons H^+, and organic bulky ammonium cations R_2N^+. The peak currents in the cyclic voltammograms (CVs) roughly correspond to negative $\Delta_o^w\phi$ such that the fractions of groups in –COOH and $–COOR_2N$ forms are both large and similar to each other. As $\Delta_o^w\phi$ is scanned more negatively from the peak, R_2N^+ ions enter the film from the organic phase and the same amount of H^+ ions are transferred from the film to the aqueous phase. Two chemical equilibria are shifted: the acid dissociation of –COOH and the exchange between bound H^+ and bound R_2N^+. For every –COOH group involved in the acid dissociation, a larger number *n* are involved in the ion exchange reaction. When –COOH dissociates, the proton H^+ is displaced to the aqueous phase by a R_2N^+ ion that enters the film to compensate for the charge of $–COO^–$. Should $\Delta_o^w\phi$ be scanned to even more negative values, the R_2N^+ concentration in the film would be so that all carboxyl groups would be in $–COOR_2N$ form and some $HCit^{2–}$ ions would enter the film to compensate for the charge of the R_2N^+ ions. Conversely, as $\Delta_o^w\phi$ is scanned from the peak to less negative values, H^+ ions enter the film from the aqueous phase and R_2N^+ ions are transferred from the film to the organic phase. Should $\Delta_o^w\phi$ be scanned to moderately positive values, Li^+ ions would enter the film to compensate for the charge of $–COO^–$. For full clarity, Scheme S1 in the Supporting Information provides another more detailed overview of the dynamics of the electrochemically-driven reversible ion intercalation process.

Results and Discussion

Electrochemistry of the floating film of ZnPor-INs at the ITIES. The film of ZnPor-INs formed at the ITIES between a lithium citrate (Li_2HCit) buffered aqueous solution and an organic solution of bis(triphenylphosphoranylidene)ammonium tetrakis(pentafluorophenyl)-borate (R_2NTB) in TFT (see cell configuration in Scheme 2). An image of the film is shown in Figure S1. The molecular liquid|liquid boundary is located within the ZnPor-IN film, which is considered as a third phase separating the aqueous and organic solutions and a mixed-solvent layer.

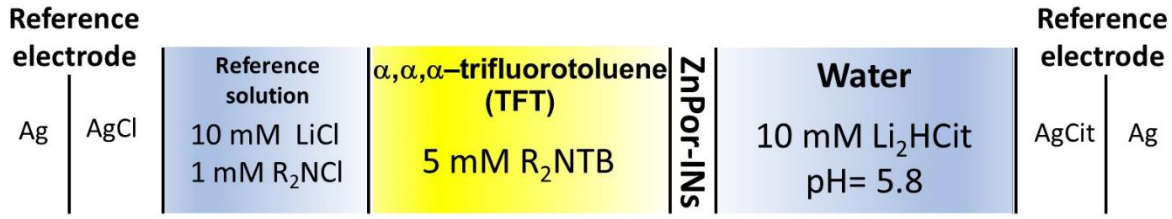

Scheme 2. The general configuration of the four-electrode cell used for electrochemical measurements at the ZnPor-IN functionalised liquid|liquid interface. The organic phase was 5 mM bis(triphenylphosphoranylidene)ammonium tetrakis(pentafluorophenyl)-borate (R_2NTB) in α,α,α-trifluorotoluene (TFT). The aqueous phase was lithium citrate (Li_2HCit) at pH 5.8 (unless otherwise stated). The ZnPor-IN films were prepared from solutions of ZnPor at concentrations in the range of 10 to 100 μM in contact with the TFT for 30 min, as described in the Experimental Section of the Supporting Information.

Cyclic voltammograms (CVs) were obtained with a four-electrode electrochemical cell, using the configuration outlined in Scheme 2, both in the absence and presence of the floating ZnPor-IN film at a scan rate of 1 $mV \cdot s^{-1}$. The interfacial concentration Γ_{ZnPor} of ZnPor in the film was determined spectroscopically (Figure S2) as described in the Experimental Section (see Supporting Information) prior to all electrochemical measurements. The control CV in the absence of film was essentially featureless (dashed line, Figure 1a). The only signal observed upon varying the applied interfacial Galvani potential difference $\Delta_o^w\phi$ was due to the aqueous background electrolyte citrate anions transferring to the organic phase at the negative extreme of the polarisable potential window (PPW). By contrast, in the presence of the ZnPor-IN film,

several electrochemical signals were observed at negative potentials (solid line, Figure 1a). The absence of redox- active species in either phase means that the electrochemical signals in the presence of the ZnPor-IN film were purely ionic in nature.

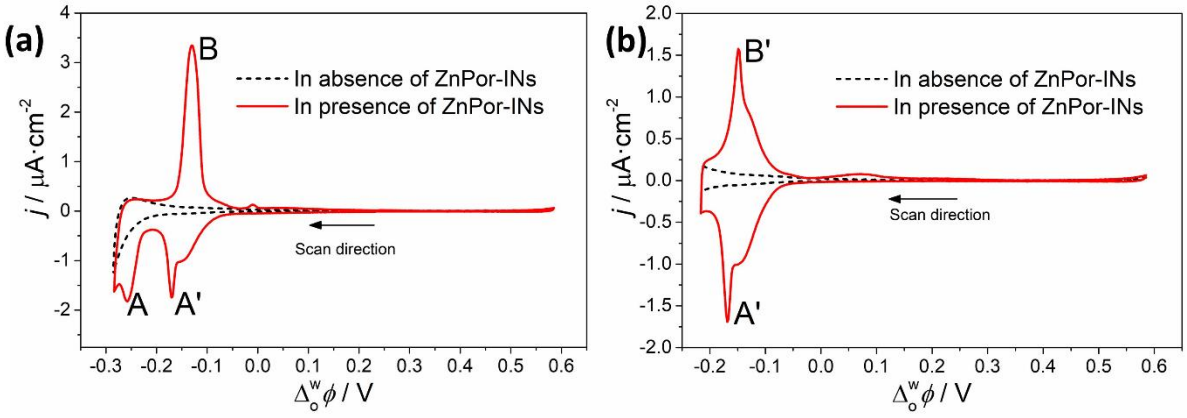

Figure 1. Cyclic voltammetry in the absence (dashed lines) and presence (solid lines) of the ZnPor-IN film at the ITIES. The electrochemical configuration of the four-electrode electrochemical cell was as described in Scheme 2. The influence of systematically varying the lower vertex potential on the CVs was investigated by switching the potential on the negative scan at **(a)** –0.285 V and **(b)** –0.215 V. The scan rate was 1 mV·s^{-1} and the start potential was 0.250 V. The interfacial concentration of ZnPor was Γ_{ZnPor} = 0.88 nmol·cm^{-2}.

The relationship between the two electrochemical signals on the negative scan with negative currents (labelled A and A' in Figure 1a) and the signal on the positive scan with a positive current (labelled B in Figure 1a) was investigated by systematically varying the lower vertex potential (Figure 1b). Switching the potential on the negative scan immediately after the appearance of peak A' lead to a major reduction in the magnitude of the electrochemical signal on the positive scan. Labelled B', this smaller peak was of a near-identical shape and magnitude to A' (Figure 1b). Therefore, the electrochemical process giving rise to peak A' was the reverse of that giving rise to peak B'. Indeed, the ratio of the magnitude of the charge for each peak was $Q_{A'}/Q_{B'} \approx 1$ for CVs obtained at scan rates ranging from 5 to 50 mV·s^{-1} and close to 0.9 V at all Γ_{ZnPor} at 1 mV·s^{-1} (Figure S3 and Tables S1 and S2). Furthermore, as peaks A and A' were related with peak B, both A and A' were associated with the same species.

The peak-to-peak separation between peaks A' and B' was 5.9 mV at a scan rate of 1 mV·s^{-1}. Additionally, the peak current i_p for peaks A' and B' varied linearly with the scan rate

(Figure S3). Thus, the kinetics of these electrochemical signals were controlled by surface processes in the presence of the ZnPor-IN film. In the electrochemical configuration described in Scheme 2, no ionic species were present capable of undergoing ion transfer across the ITIES within the PPW. Therefore, the electrochemical signals observed in the presence of the ZnPor-IN film were due to a diffusion-less process, *i.e.*, adsorption and capacitive phenomena, and not Faradaic ion transfer.

Self-assembly of the floating ZnPor-IN film at the ITIES was optimal at pH 5.8.[36] As this pH matched the pK_a of the ZnPor carboxyl groups, statistically 50% of them were deprotonated and charged in the bulk aqueous solution. Differential capacitance measurements are a macroscopic view of the charge distribution of the back-to-back diffusion layer or mixed solvent region.[23,37–41] The capacitance minimum appears at the potential of zero charge (PZC). Figure 2a shows differential capacitance measurements obtained in the presence and absence of the ZnPor-IN film. Capacitance values were calculated from the imaginary part of the impedance at a frequency of 80 Hz. This frequency was selected in order to suppress Faradaic contributions due to ion transfer within the PPW. This effect was demonstrated in Figure S4a where the Faradaic current due to ion transfer of tetraethylammonium cations across a bare water|TFT interface was entirely filtered out at 80 Hz. A shift in the PZC of +100 mV was observed in the presence of the ZnPor-IN film (Figure 2a). This shift confirms a negative excess charge at the interface due to presence of deprotonated carboxyl groups at this pH.[36] The peak at –0.15 V was seen at all frequencies across a range from 5 to 80 Hz (Figure S4b), further confirming that these electrochemical signals in the presence of the ZnPor-IN film were associated with adsorption and capacitive processes.

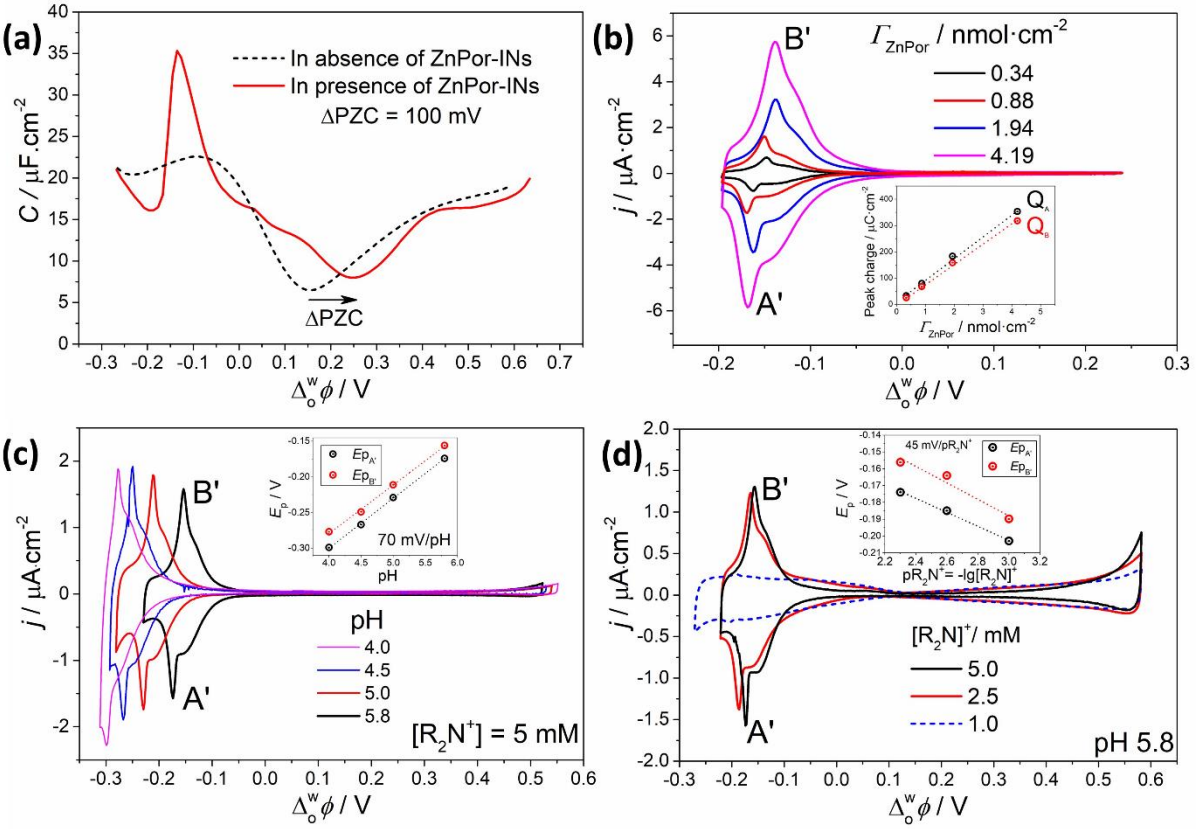

Figure 2. (a) Monitoring the potential of zero charge (PZC) by obtaining differential capacitance curves in the absence (dashed line) and presence (solid line) of the ZnPor-IN film. The capacitance was calculated from impedance measurements every 5 mV at 80 Hz assuming an *RC* circuit where *R* represents the solution resistance and *C* the double-layer capacitance. Γ_{ZnPor} determined spectroscopically as 0.34 nmol·cm^{-2}. **(b)** Cyclic voltammetry in the presence of ZnPor-IN films of increasing Γ_{ZnPor}. The scan rate used was 1 mV·s^{-1}. Inset: dependence of the peak charge *Q* on Γ_{ZnPor}. The effect of varying **(c)** the pH and **(d)** R_2NTB concentration on the electrochemical response was investigated in the presence of the ZnPor-IN film. The scan rate used was 5 mV·s^{-1} and Γ_{ZnPor} was 0.34 nmol·cm^{-2}. Insets in **(c)** and **(d)**: the relationships between peak potential E_p and pH or pR_2N^+ (= –lg [R_2N^+]), respectively. For clarity, a zoomed in version of the CV obtained with [R_2N^+] = 1 mM (dashed blue line) in **(d)** is shown in Figure S6.

The electrochemical signals in Figure 1 appear at negative $\Delta_o^w\phi$, suggesting the binding of R_2N^+ cations to the carboxyl groups of the ZnPor. These groups may exist in three states: –COO^-, –COOH and –$COOR_2N$. Their concentrations c_{COO^-}, c_{COOH} and c_{COOR_2N} can vary with

the bulk aqueous pH, the applied $\Delta_o^w\phi$, as well as with the Li_2HCit and R_2NTB concentrations. On the contrary, the total concentration

$$c_{T,COO} = c_{COO^-} + c_{COOH} + c_{COOR_2N} \qquad (1)$$

is a constant related to Γ_{ZnPor}. To corroborate the relation with $c_{T,COO}$, Γ_{ZnPor} was systematically varied by increasing the bulk aqueous ZnPor concentration during the ZnPor-IN film self-assembly. A linear increase in the charge for each peak, $Q_{A'}$ and $Q_{B'}$, was observed (Figure 2b). This linear increase was obtained despite Γ_{ZnPor} far exceeding that expected for an interfacial monolayer of ZnPor (estimated as 0.095 nmol·cm^{-2}, see Figure S5). Thus, the electrochemical signals were due to processes involving carboxyl groups within the ZnPor-IN film, and not only at surface sites facing the aqueous and organic electrolytes.

To probe the effects of the bulk aqueous pH and R_2N^+ concentration, both were varied independently (Figures 2c and d). As we described previously,[36] the ZnPor-INs were stabilised by cooperative hydrogen bonding. Thus, pH conditions more alkali than the carboxyl groups pK_a of 5.8 were ruled out as the ZnPor-IN film would destabilise and dissolve. The peak potentials for peaks A' ($E_{pA'}$) and B' ($E_{pB'}$) were found to depend on both the pH and pR_2N^+ (where $pR_2N^+ = -\lg [R_2N^+]$), confirming their role in the electrochemical processes occurring at the ZnPor-IN functionalised ITIES. Uniform shifts of –70 mV/pH and +45 mV/pR_2N^+ were observed for both $E_{pA'}$ and $E_{pB'}$ (insets, Figures 2c and d). The magnitude of peaks A' and B' decreased drastically at the lowest R_2N^+ concentration investigated ($[R_2N^+]$ = 1 mM), Figure 2d and Figure S6.

The influence of the nature of the aqueous anion on the electrochemical response was also investigated. Citrate anions are sensitive to pH, with pK_a's at 3.13, 4.76 and 6.40, respectively.[42] Thus, as the pH at the ITIES varies as a function of applied $\Delta_o^w\phi$, a pH insensitive anion was chosen for comparison by replacing Li_2HCit with LiCl. As shown in Figure S7, the nature of the anion had minimal effect on the electrochemical response. A near identical CV shape was observed and the trend in the shifts of $E_{pA'}$ and $E_{pB'}$ with pH replicated.

Peaks A' and B' in the CVs in Figures 1 and 2b-d are formed by the superposition of a narrow peak and a broad peak. Narrow "adsorption" peaks in CVs are considered to indicate positive cooperativity, *i.e.,* every adsorption event is facilitated by the occurrence of a previous adsorption event. In this regard, for fundamental thermodynamic reasons, the CVs can be described using the Frumkin isotherm.[15] For peak B', we attribute the broad shoulders to binding of R_2N^+ at $–COO^–$ groups and ion exchange of R_2N^+ with –COOH groups (in which

protons are displaced) near the o|IN interface as R_2N^+ flows from the organic phase into the ZnPor-IN film. The sharp peak of B' is attributed to binding and ion exchange of R_2N^+ at $–COO^–$ and –COOH groups, respectively, deeper inside the ZnPor-IN film. The second electrochemical signal on the negative scan, peak A, is attributed to a second binding and ion exchange event inside the ZnPor-IN film requiring more electrochemical driving force (see Figure 1a). As detailed in the following section, all peaks are capacitive in nature and resemble "adsorption" due to a saturation limit to the concentration of $–COOR_2N$ species that form by binding and ion exchange as $\Delta_o^w\phi$ is scanned negatively.

Modelling of electrochemically-driven reversible ion intercalation in the presence of the ZnPor-IN film. The modelling aims to clarify: (i) the capacitive nature of the electrochemical signals at negative $\Delta_o^w\phi$ in the presence of the ZnPor-IN film, (ii) the trends in the shifts of the peak potentials as a function of the bulk aqueous pH and R_2N^+ concentration, and (iii) the characteristic CV shapes indicative of positive cooperativity. For the electrolyte concentrations used in the electrochemical experiments, the film thickness, $L^{IN} \approx 100$ nm,[36] is much larger than the aqueous and organic Debye lengths and the molecular liquid|liquid boundary is located within the ZnPor-IN film. Thus, as the film is considered as an intermediate phase (IN) separating the aqueous (w) and organic (o) solutions. From the point of view of ion solvation, it is a mixed-solvent layer, disliked by both aqueous ions and organic ions.

Within the PPW, no ions can transfer across the ITIES and the ZnPor-IN film behaves as a capacitor (Scheme 3). When $\Delta_o^w\phi$ is scanned progressively more negative, the R_2N^+ ions are "pushed" into the film, but cannot transfer to the aqueous phase. Then, a few –COOH groups are forced to dissociate, and many more transform into $–COOR_2N$. In both cases, the released H^+ ions are "pulled" into the aqueous phase. The charge of the anionic carboxyl groups $–COO^–$ is mostly compensated by R_2N^+, which are the majority ions in the film; $HCit^{2–}$ and Li^+ are present only when $\Delta_o^w\phi$ is very different to that around the peaks in Figure 2b. To understand the behaviour of the film as a capacitor, carboxyl groups in –COOH form are taken as a reference corresponding to absence of charges in the capacitor "plates". The positive plate accumulates charge in the form of free R_2N^+ and bound R_2N^+. That is, the charge q^o in this positive plate is basically proportional to $c_{COOR_2N} + c_{R_2N}^{IN}$. The negative plate has a charge $q^w < 0$ which is a measure of the reduction in the amount of –COOH groups, and hence proportional to $c_{T,COO} - c_{COOH}$. As $\Delta_o^w\phi$ is made more negative, $q^o = -q^w > 0$ increases, but remains of the order of $c_{T,COO}$. The unfavourable solvation in this mixed-solvent layer bounds

the free ion concentrations $c^{\mathrm{IN}}_{\mathrm{R_2N}}$ and $c^{\mathrm{IN}}_{\mathrm{HCit}}$ to relatively small values, even for the most negative $\Delta^{\mathrm{w}}_{\mathrm{o}}\phi$.

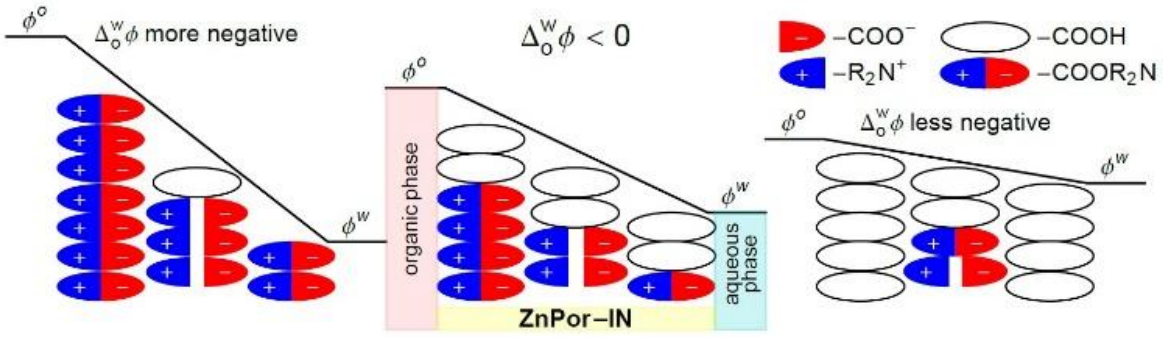

Scheme 3. The ZnPor-IN functionalised liquid|liquid interface behaves as a capacitor. Carboxyl groups in –COOH form are taken as a reference corresponding to absence of charges in the capacitor "plates". When $\Delta^{\mathrm{w}}_{\mathrm{o}}\phi$ is scanned progressively negative, the R_2N^+ ions are "pushed" into the film, a few –COOH groups are forced to dissociate, and many more transform into $–COOR_2N$. The released H^+ ions are "pulled" into the aqueous phase.

The concentrations of the ionic species R_2N^+, TB^-, $HCit^{2-}$, H^+ and Li^+ in the film (phase IN) must satisfy the local electroneutrality condition

$$c_{\mathrm{COO^-}} + 2c^{\mathrm{IN}}_{\mathrm{HCit}} + c^{\mathrm{IN}}_{\mathrm{TB}} = c^{\mathrm{IN}}_{\mathrm{R_2N}} + c^{\mathrm{IN}}_{\mathrm{Li}} + c^{\mathrm{IN}}_{\mathrm{H}} \qquad (2)$$

The local electroneutrality condition can also be presented as $q^{\mathrm{o}} + q^{\mathrm{w}} = 0$ where

$$q^{\mathrm{o}} = FL^{\mathrm{IN}}\left(c_{\mathrm{COOR_2N}} + c^{\mathrm{IN}}_{\mathrm{R_2N}} - c^{\mathrm{IN}}_{\mathrm{TB}}\right) \qquad (3)$$

$$-q^{\mathrm{w}} = FL^{\mathrm{IN}}\left(c_{\mathrm{T,COO}} - c_{\mathrm{COOH}} + 2c^{\mathrm{IN}}_{\mathrm{HCit}} - c^{\mathrm{IN}}_{\mathrm{H}} - c^{\mathrm{IN}}_{\mathrm{Li}}\right) \qquad (4)$$

are the charge densities in the capacitor and F is Faraday's constant. In the potential range $-0.25\ \mathrm{V} < \Delta^{\mathrm{w}}_{\mathrm{o}}\phi < -0.05\ \mathrm{V}$, the concentrations of R_2N^+, $HCit^{2-}$ and $–COO^-$, $c^{\mathrm{IN}}_{\mathrm{R_2N}}$, $c^{\mathrm{IN}}_{\mathrm{HCit}}$ and $c^{\mathrm{IN}}_{\mathrm{COO^-}}$, are the dominant terms in Equation (2). For $\Delta^{\mathrm{w}}_{\mathrm{o}}\phi > -0.05\ \mathrm{V}$, the concentrations $c^{\mathrm{IN}}_{\mathrm{Li}}$ and $c^{\mathrm{IN}}_{\mathrm{TB}}$ of the Li^+ and TB^- species may become significant. Although some species make a negligible contribution in Equation (2), we keep them all for the sake of generality. The electrical double layers at the o|IN and IN|w interfaces extend over a fraction of the film thickness L^{IN}, and local electroneutrality does not hold there. However, the contributions of the

associated interfacial capacitances are small compared to other effects described below and, therefore, can be neglected.

The concentrations of the ionic species in phase IN are different from those in their respective phases. In absolute value, the Gibbs energy of transfer of the organic ions from phase o to phase IN is intermediate to that from phase o to phase w. Similarly, in absolute value, the Gibbs energy of transfer of the aqueous ions from phase w to phase IN is intermediate to that from phase w to phase o. Therefore, the ions have no chemical preference to enter phase IN, and their chemical partition coefficients into this phase are significantly lower than unity, $P_i \ll 1$. The applied potential $\Delta_{\mathrm{o}}^{\mathrm{w}}\phi$ also affects the distribution of the ions. The potential ϕ^{IN} is usually intermediate between those phases w and o, so that $\Delta_{\mathrm{IN}}^{\mathrm{w}}\phi = \phi^{\mathrm{w}} - \phi^{\mathrm{IN}}$, $\Delta_{\mathrm{o}}^{\mathrm{IN}}\phi = \phi^{\mathrm{IN}} - \phi^{\mathrm{o}}$ and

$$\Delta_{\mathrm{o}}^{\mathrm{w}}\phi = \Delta_{\mathrm{IN}}^{\mathrm{w}}\phi + \Delta_{\mathrm{o}}^{\mathrm{IN}}\phi \qquad (5)$$

have the same sign. The distribution equilibrium of, *e.g.*, the organic cation R_2N^+ between phases o and IN requires $c_{\mathrm{R_2N}}^{\mathrm{IN}} = c^{\mathrm{o,b}} P_{\mathrm{R_2N}} \mathrm{e}^{-f\Delta_{\mathrm{o}}^{\mathrm{IN}}\phi}$ where $c^{\mathrm{o,b}} = [\mathrm{R_2N^+}]$ is its concentration in the bulk organic phase. Similar equations can be formulated for the other species, as described in detail in the Supporting Information.

The evaluation of the concentrations $c_{\mathrm{COO^-}}$, c_{COOH} and $c_{\mathrm{COOR_2N}}$ in Equations (2)-(4) require the simultaneous consideration of the ionic distribution equilibria and the chemical equilibria. Since $c_{\mathrm{H}}^{\mathrm{IN}} = c_{\mathrm{H}}^{\mathrm{w,b}} P_{\mathrm{H}} \mathrm{e}^{f\Delta_{\mathrm{IN}}^{\mathrm{w}}\phi}$, both the negative $\Delta_{\mathrm{o}}^{\mathrm{w}}\phi$ and the mixed-solvent nature of phase IN contribute to increase the interfacial pH with respect to the bulk aqueous pH, $\mathrm{pH}^{\mathrm{IN}} - \mathrm{pH} = -\lg\left(c_{\mathrm{H}}^{\mathrm{IN}}/c_{\mathrm{H}}^{\mathrm{w,b}}\right) > 0$. Yet, if the latter is equal or lower than the $\mathrm{p}K_{\mathrm{a}} = 5.8$ of the carboxyl groups, some of these groups can be protonated according to the equilibrium

$$K_{\mathrm{a}}^{\mathrm{IN}} c^{\circ} = \frac{c_{\mathrm{H}}^{\mathrm{IN}} c_{\mathrm{COO^-}}}{c_{\mathrm{COOH}}} \qquad (6)$$

where $c^{\circ} = 1\ \mathrm{M}$ and $K_{\mathrm{a}}^{\mathrm{IN}} = K_{\mathrm{a}} P_{\mathrm{H}}$, see Equation (S32) in the Supporting Information. The abundant R_2N^+ cations in phase IN can displace the bound protons and form –$COOR_2N$ groups. The equilibrium of the ion exchange reaction

$$-\mathrm{COOH(IN)} + \mathrm{R_2N^+(IN)} \rightleftarrows -\mathrm{COOR_2N(IN)} + \mathrm{H^+(IN)} \qquad (7)$$

requires

$$K_{\mathrm{IE}}^{\circ,\mathrm{IN}} = \frac{c_{\mathrm{H}}^{\mathrm{IN}} c_{\mathrm{COOR_2N}}}{c_{\mathrm{R_2N}}^{\mathrm{IN}} c_{\mathrm{COOH}}} \qquad (8)$$

where $K_{\mathrm{IE}}^{\circ,\mathrm{IN}}$ is the equilibrium constant. From Equations (1), (6) and (8), the fraction of charged carboxyl groups is

$$\frac{c_{\mathrm{COO^-}}}{c_{\mathrm{T,COO}}} = \frac{K_{\mathrm{a}}^{\mathrm{IN}} c^{\circ}}{K_{\mathrm{a}}^{\mathrm{IN}} c^{\circ} + c_{\mathrm{H}}^{\mathrm{IN}} + K_{\mathrm{IE}}^{\circ,\mathrm{IN}} c_{\mathrm{R_2N}}^{\mathrm{IN}}} \qquad (9)$$

Substituting $c_{\mathrm{COO^-}}$ from Equation (9) into Equation (2), and using the conditions of distribution equilibria of the ionic species, the potential drop $\Delta_{\mathrm{IN}}^{\mathrm{w}}\phi$ can be determined, see Equation (S17) in the Supporting Information. Hence, the ionic concentrations and q^{o} are known as functions of $\Delta_{\mathrm{o}}^{\mathrm{w}}\phi$, as well as the differential capacitance of the ZnPor-IN film

$$C = -\mathrm{d}q^{\mathrm{o}}/\mathrm{d}\Delta_{\mathrm{o}}^{\mathrm{w}}\phi \qquad (10)$$

The applied potential $\Delta_{\mathrm{o}}^{\mathrm{w}}\phi$ affects the distribution of the ions, and hence also the ion exchange equilibrium. Thus, Equation (8) can be transformed to

$$\frac{c_{\mathrm{COOR_2N}}}{c_{\mathrm{COOH}}} = K_{\mathrm{IE}}^{\circ,\mathrm{IN}} \frac{c^{\mathrm{o,b}} P_{\mathrm{R_2N}}}{c_{\mathrm{H}}^{\mathrm{w,b}} P_{\mathrm{H}}} \mathrm{e}^{-f\Delta_{\mathrm{o}}^{\mathrm{w}}\phi} \qquad (11)$$

As $\Delta_{\mathrm{o}}^{\mathrm{w}}\phi$ is scanned progressively negative, $q^{\mathrm{o}} = -q^{\mathrm{w}} > 0$ increases. Across the IN|w interface, $\mathrm{HCit^{2-}}$ ions may flow from phase w into phase IN (if $\Delta_{\mathrm{o}}^{\mathrm{w}}\phi$ is sufficiently negative); the flow of $\mathrm{Li^+}$ and $\mathrm{H^+}$ ions from phase IN to phase w is usually negligible. Across the o|IN interface, $\mathrm{R_2N^+}$ ions flow into phase IN; the flow of $\mathrm{TB^-}$ ions from phase IN to phase o is usually much smaller. The increase in $c_{\mathrm{R_2N}}^{\mathrm{IN}} = c^{\mathrm{o,b}} P_{\mathrm{R_2N}} \mathrm{e}^{-f\Delta_{\mathrm{o}}^{\mathrm{IN}}\phi}$ shifts the ion exchange equilibria towards the formation of –$\mathrm{COOR_2N}$, at the expense of reducing $c_{\mathrm{COO^-}}$ and c_{COOH}. The increase in $c_{\mathrm{COOR_2N}}$ gives rise to an "adsorption" peak in the CV because there is a saturation limit, $c_{\mathrm{COOR_2N}} \leq c_{\mathrm{T,COO}}$. By convention, a positive charge flow from o to w gives rise to a peak in the CV of negative current.[20,21] Similarly, as $\Delta_{\mathrm{o}}^{\mathrm{w}}\phi$ is made more positive, $q^{\mathrm{w}} = -q^{\mathrm{o}} > 0$ increases. Across the o|IN interface, $\mathrm{R_2N^+}$ ions flow towards phase o. Across the IN|w interface, $\mathrm{HCit^{2-}}$ ions flow towards phase w. During such a potential scan, $c_{\mathrm{COOR_2N}}$ decreases as $c_{\mathrm{COO^-}}$ and c_{COOH} increase. The increase in $c_{\mathrm{COO^-}}$ gives rise to an "adsorption" peak with a positive current in the CV (negative charge flow from o to w).

The CVs can be simulated using an equivalent electrical circuit consisting of the solution resistance R_{sol} in series with the parallel combination of the film capacitance *C* and the charge transfer resistance R_{ct} (see Equations S19 and S20, Supporting Information). This simple theoretical model qualitatively captures the main features of the experimental CVs, such as the total charge under the peaks, the peak separation and their variation with the bulk aqueous

pH and the organic electrolyte concentration (see Figure 3 and Tables S3 and S4). However, this model does not accurately reproduce the shape of the peaks. The experimental peaks are the superposition of a narrow peak and a broad peak, the former occurring at a more negative $\Delta_o^w\phi$ and having a smaller area (and hence charge) under the peak. Even the broad peak is narrower than predicted by this model.

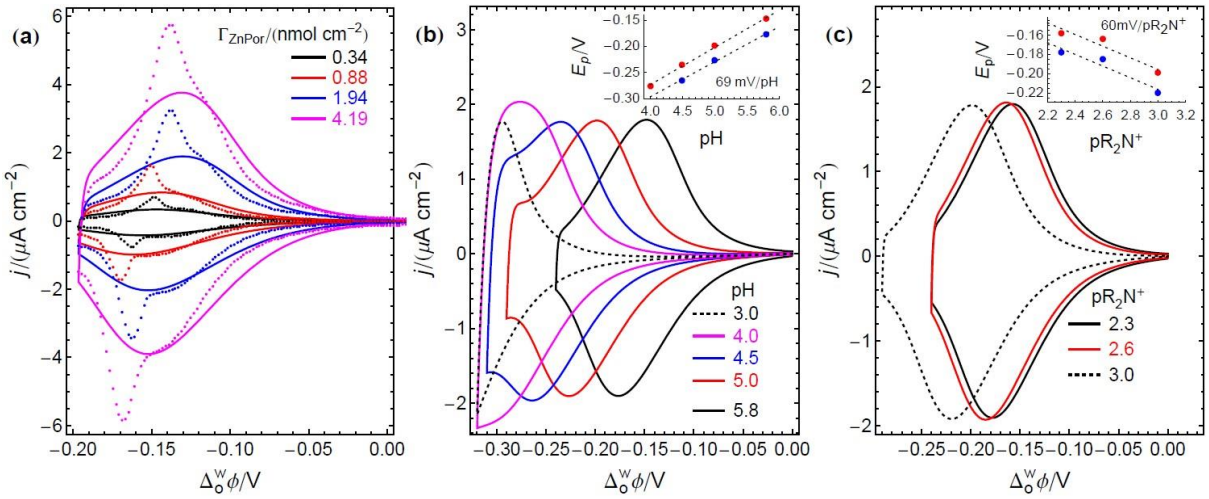

Figure 3. CVs generated using the theoretical model qualitatively capture the main features of the experimental CVs at the ITIES in the presence of a ZnPor-IN film. **(a)** A comparison of the simulated (lines) and experimental CVs (symbols) at 1 mV·s^{-1} for the electrochemical cell described in Scheme 2 (with 5 mM R_2NTB, 10 mM Li_2HCit, a bulk aqueous pH = 5.8 and varying Γ_{ZnPor}). In particular, the peak separation and the total charge under the peaks are well reproduced, though the shape of the peaks is not. The simulated CVs accurately describe the experimentally observed values of peak potentials and their linear shift with **(b)** the pH and **(c)** the R_2NTB concentration at 5 mV·s^{-1} and Γ_{ZnPor} = 0.34 nmol·cm^{-2}. The parameter values for the simulations in panels (a)-(c) are shown in Tables S3 and S4.

Narrow "adsorption" peaks in the CVs are considered an indication of positive cooperativity. Herein, we propose that once the initial bulky R_2N^+ cations flow across the o|IN interface as $\Delta_o^w\phi$ is scanned negatively, they "open" space in the nanostructure due to structural rearrangements of the porphyrins allowing the later R_2N^+ species to penetrate the ZnPor-IN film much more easily. Thus, this conformational change of the ZnPor-INs is the physical reason behind the negative g interaction parameters discussed *vide infra*, that is characteristic of positively cooperative adsorption. Furthermore, the characteristic shape of the purely

capacitive CVs due to structural rearrangements of the porphyrins at the electrified liquid|liquid interface precisely resemble those of systems involving phase transitions at electrified solid|liquid interfaces, for example electrochemically driven structural changes of a copper adlayer on a Au(111) electrode surface.[43]

Cooperative binding of R_2N^+ ions can be described using the Frumkin isotherm, described in detail in the Supporting Information. As mentioned above, the peaks in the experimental CVs are formed by the superposition of a narrow peak and a broad peak. Accordingly, we have simulated the CV by adding the theoretical curves calculated with two sets of carboxyl groups, described by Equation (S24) in the Supporting Information. The set responsible for the narrow peak has a more negative Frumkin parameter g_{narrow} and a smaller constant $K^{\circ,\mathrm{IN}}_{\mathrm{IE,narrow}}$, so that the peak appears at more negative $\Delta^{\mathrm{w}}_{\mathrm{o}}\phi$, compared to the less negative g_{broad} and larger $K^{\circ,\mathrm{IN}}_{\mathrm{IE,broad}}$ corresponding to the set responsible for the broad peak. The electrical parameters R_{sol} and R_{ct} in Equation (S20), Supporting Information, are common to both sets (Table S5). At 298 K, $g_{\mathrm{narrow}} = -3.5$ and $g_{\mathrm{broad}} = -0.7$ correspond to attractive interaction energies $z_{\mathrm{c}}\varepsilon_{\mathrm{narrow}} = g_{\mathrm{narrow}}RT = -8.67\ \mathrm{kJ \cdot mol^{-1}}$ and $g_{\mathrm{broad}}RT = -1.73\ \mathrm{kJ \cdot mol^{-1}}$. These g values seem reasonable on the basis of the excellent agreement (Figures 4 and S7) between the simulated and the experimental CVs, given the complexity of the system under consideration. Moreover, a value $g = -4.2$ was observed for a Li^+ intercalation process, a system with very similar underlying thermodynamics.[13]

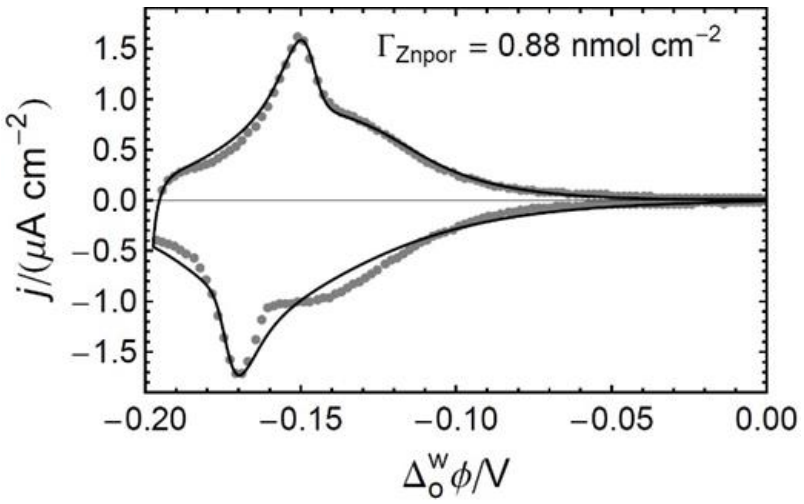

Figure 4. The consideration of two types of binding sites, described by Equation (S24), Supporting Information, with $g_{\mathrm{narrow}} = -3.5$ and $g_{\mathrm{broad}} - 0.7$, predicts simulated CVs

(lines) at 1 mV·s^{-1} and Γ_{ZnPor} = 0.88 nmol·cm^{-2} that resemble more closely the experimental observations (symbols). Comparisons are provided for CVs obtained with Γ_{ZnPor} values of 0.34, 1.94 and 4.19 nmol·cm^{-2} in Figure S8. The parameter values (Table S5) have been chosen on the basis of a qualitative agreement and not using a fitting algorithm.

Kinetics of electrochemically-driven reversible ion intercalation in the presence of the ZnPor-IN film. As $\Delta_{\mathrm{o}}^{\mathrm{w}}\phi$ is scanned progressively negative, ion intercalation of R_2N^+ from the organic phase into the ZnPor-IN film proceeds by binding and ion exchange, with $c_{\mathrm{COOR_2N}}^{\mathrm{IN}}$ increasing. The aim of this section is to investigate the kinetics of this process by potential-step chronoamperometry. A particular focus is placed on the influence of both $\Delta_{\mathrm{o}}^{\mathrm{w}}\phi$ and Γ_{ZnPor} on the rates of the charge transfer processes. Current transients were obtained by maintaining a constant initial potential $\Delta_{\mathrm{o}}^{\mathrm{w}}\phi_{\mathrm{initial}}$ for $t_{\mathrm{initial}} = 30$ s, and varying the final potential $\Delta_{\mathrm{o}}^{\mathrm{w}}\phi_{\mathrm{final}}$ in 50 mV increments across the region where the electrochemical signals were observed ($-0.05\ \mathrm{V} > \Delta_{\mathrm{o}}^{\mathrm{w}}\phi > -0.30\ \mathrm{V}$), see Figure S9 and Figures 5a-b. The value $\Delta_{\mathrm{o}}^{\mathrm{w}}\phi_{\mathrm{initial}} = +0.25$ V was chosen because no discernible electrochemical processes were occurring at that $\Delta_{\mathrm{o}}^{\mathrm{w}}\phi$, besides capacitive charging of the back-to-back double layers at the ITIES. Once more, four electrochemical cells with increasing Γ_{ZnPor} (0.34, 0.88, 1.94, and 4.19 nmol·cm^{-2}) were investigated.

Depending on $\Delta_{\mathrm{o}}^{\mathrm{w}}\phi_{\mathrm{final}}$ and Γ_{ZnPor}, the current transients presented a decay component, commonly associated to an adsorption process, and multiple rising components with current maxima, commonly associated with nucleation and growth processes. In this regard, these current transients obtained by potential-step chronoamperometry are highly reminiscent of those generated using the same technique to study the kinetics of structural changes during the electrochemical switching of electronically conducting polymer films, such as polypyrrole, between their reduced (insulating) and oxidised (electronically conducting) states.[35] The kinetics of processes in conducting polymers that lead to a current maximum after a potential-step are described by the electrochemically stimulated conformational relaxation (ESCR) model.[44,45] In common with conducting polymer films, electrochemically driven processes (binding and ion exchange)in the ZnPor-IN film occur throughout a three-dimension volume, with ion intercalation steps linked to morphological changes in the film structures.

A key question is how do we define the meaning of "nucleation" in the context of the ZnPor-IN film at the ITIES? Herein, we propose that the presence of nucleation transients was

associated with domains within the nanostructures where, due to structural rearrangements of the porphyrins, the binding and ion exchange of R_2N^+ at $–COO^–$ and –COOH groups, respectively, took place faster. Also, the energetically less demanding binding and ion exchange of further R_2N^+ species after these structural rearrangements of the porphyrins is the physical reason underlying the electrochemical observation of positively cooperative behaviour discussed earlier.

Prior to kinetic analysis, the initial 50 ms (the value obtained from impedance measurements for the RC constant of the cell) were neglected and the residual current subtracted such that $j = 0$ A·cm^{-2} at $t = 40$ s. For all Γ_{ZnPor} values, the transients obtained using –0.05 V, –0.10 V and –0.15 V as $\Delta_o^w\phi_{\mathrm{final}}$ (and +0.25 V as $\Delta_o^w\phi_{\mathrm{initial}}$) did not show any significant nucleation component (Figure S9). Thus, the analysis was focused on the transients obtained using –0.25 V, –0.30 V and –0.35 V as $\Delta_o^w\phi_{\mathrm{final}}$, where the nucleation features were observed (Figures 5a-b). In many cases, more than one nucleation component was observed experimentally, up to a maximum of three. The latter may be associated with binding and ion exchange at inner carboxyl sites. Therefore, the nucleation components were de-convoluted from the total current signal by plotting the derivative of the total current. From the derivative, the time t_{max} of the peak current maximum for each nucleation component within each transient was easily identified, see Figure 5c. A summary of these t_{max} values as a function of Γ_{ZnPor} and $\Delta_o^w\phi_{\mathrm{final}}$ is presented in Table S6. Using these t_{max} values as a clear guide to the number of nucleation components present, the total fitted current for any transient may be obtained as a summation of the adsorption and nucleation components using exponential decay and Gaussian-type functions, respectively (Figure S10).

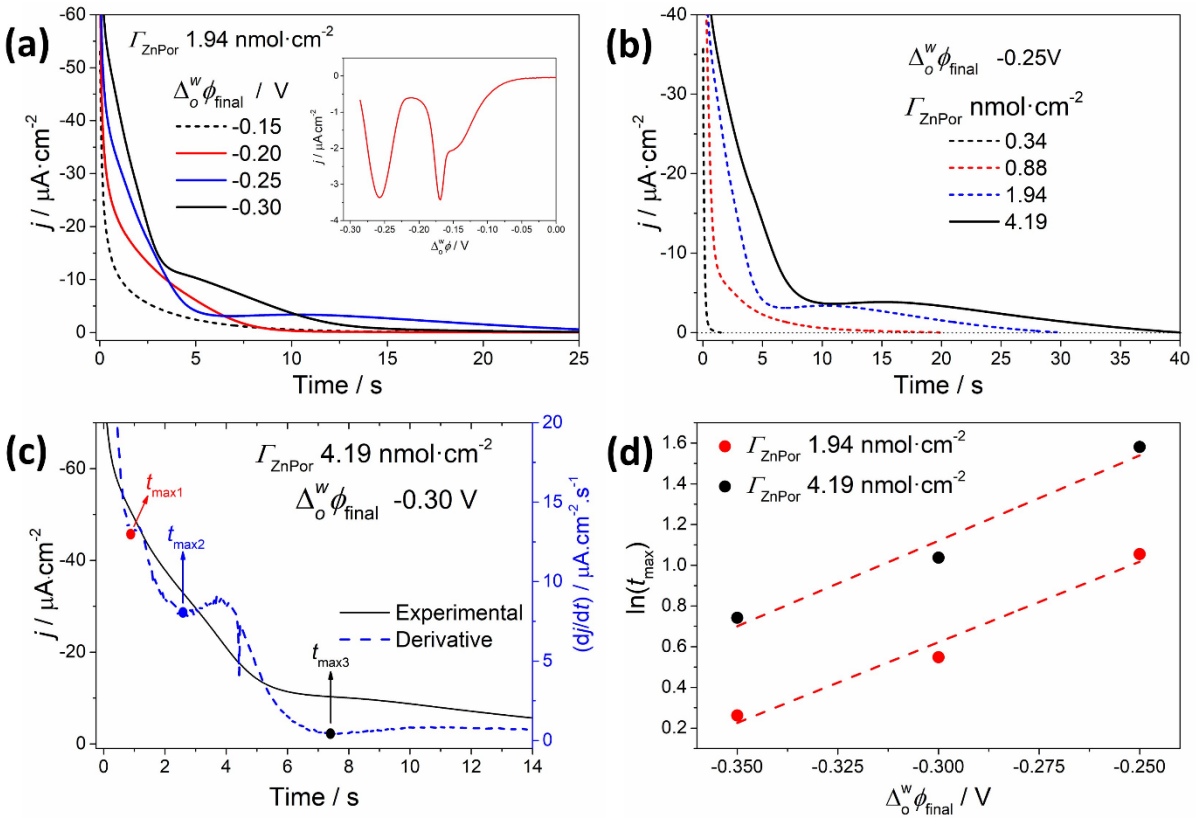

Figure 5. Kinetics of electrochemically-driven reversible ion intercalation by potential-step chronoamperometry in the presence of the ZnPor-IN film. **(a)** Current transients probing the influence of $\Delta_o^w\phi_{final}$ were obtained by varying $\Delta_o^w\phi_{final}$ in 50 mV increments at a constant Γ_{ZnPor} of 1.94 nmol·cm^{-2} and $\Delta_o^w\phi_{initial}$ of +0.25 V for 30 s ($t_{initial}$). **(b)** Current transients probing the influence of Γ_{ZnPor} were obtained by increasing Γ_{ZnPor} from 0.34 to 4.19 nmol·cm^{-2} while maintaining a constant $\Delta_o^w\phi_{initial}$ of +0.25 V for 30 s and $\Delta_o^w\phi_{final}$ of –0.25 V. **(c)** Deconvolution of the t_{max} values of the nucleation components from an experimental current transient (solid black line, obtained with a Γ_{ZnPor} of 4.19 nmol·cm^{-2}, $\Delta_o^w\phi_{initial}$ of +0.25 V for 30 s, and $\Delta_o^w\phi_{final}$ of –0.30 V) by obtaining the derivative (dashed blue line). **(d)** Plot of ln(t_{max}/s) *versus* $\Delta_o^w\phi_{final}$ for current transients obtained with a $\Delta_o^w\phi_{initial}$ of +0.25 V for 30 s and Γ_{ZnPor} of either 1.94 (red circles) or 4.19 nmol·cm^{-2} (black circles). The t_{max} data is that obtained for the second nucleation component, designated as t_{max2} in Table S6.

An increase in nucleation kinetics will be reflected in a shorter time required to reach t_{max} for each nucleation component. For all values of Γ_{ZnPor} and $\Delta_o^w\phi$, the shifts of t_{max} followed consistent trends. At a constant Γ_{ZnPor} and $\Delta_o^w\phi_{initial}$, an increase in nucleation kinetics (decreasing t_{max}) was seen as $\Delta_o^w\phi_{final}$ was set to more negative values (Figure 5a and Table

S6). In other words, conformational relaxation to the more open nanostructure is faster as more energy is applied to drive R_2N^+ species into the ZnPor-IN film, leading to the creation of more nuclei. Conversely, at a constant $\Delta_o^w\phi_{initial}$ of +0.25 V and $\Delta_o^w\phi_{final}$ of –0.25 V, a decrease in nucleation kinetics (increasing t_{max}) was seen as Γ_{ZnPor} increased (Figure 5b and Table S6). The latter indicates that more energy is required to achieve conformational relaxation as Γ_{ZnPor} increases. A prediction of the ESCR model is that a linear relationship exists between $\ln(t_{max}/s)$ and the energy required to relax and swell the conducting polymer film by oxidation, *i.e.* the anodic overpotential.[46] In line with this prediction, plots of $\ln(t_{max}/s)$ *versus* $\Delta_o^w\phi_{final}$ for one of the nucleation sites (designated t_{max2}) are linear and exhibit the same slope for the higher Γ_{ZnPor} studied, 1.94 and 4.19 nmol·cm^{-2} (Figure 5d). The latter identical slopes indicate the rate of increase in nucleation kinetics (decreasing t_{max}) as $\Delta_o^w\phi_{final}$ shifts negatively is independent of Γ_{ZnPor} in the range studied, highlighting that the liquid-liquid interface buried within the nanostructure has a finite thickness.

Finally, the effect of the initial "compaction" of the ZnPor-IN film on the kinetics were evaluated using two different experimental approaches. As R_2N^+ are bulky organic cations, far larger than the protons they displace from –COOH groups, it can be reasonably assumed that the volume of the ZnPor-IN film swells at negative $\Delta_o^w\phi$ values, reducing the films compaction. First, Γ_{ZnPor} and $\Delta_o^w\phi_{final}$ were maintained constant at 1.94 nmol·cm^{-2} and –0.25 V, respectively, and $\Delta_o^w\phi_{initial}$ varied from +0.20 V to +0.45 V every 50 mV with a $t_{initial}$ of 30 s (Figure S11a). The current transients measured were near identical for all values of $\Delta_o^w\phi_{initial}$ tested with no measurable difference in the absorption component and, on close inspection (see inset Figure S11a), a slight decrease of t_{max} for the prominent nucleation component. This slight increase in the nucleation kinetics is the opposite of what was expected if the film was more compact at positive values of $\Delta_o^w\phi_{initial}$. We attribute the minor increase in nucleation kinetics to an interaction of the organic anions, TB^-, with the ZnPor-IN film at positive potentials leading to a partial opening of the nanostructure. As the ZnPor-IN film and TB^- are both negatively charged, this interaction is far weaker than that of ZnPor-IN film and the R_2N^+ species. Nevertheless, when the potential is stepped to –0.25 V, slightly less energy is required to open space for the penetration of the R_2N^+ species. In the second experiment, Γ_{ZnPor}, $\Delta_o^w\phi_{initial}$, and $\Delta_o^w\phi_{final}$ were maintained constant at 1.94 nmol·cm^{-2}, +0.25 V and –0.25 V respectively, and $t_{initial}$ varied from 5 to 60 s (Figure S11b). As for the previous experiment, the current transients measured were near identical for all values of $t_{initial}$ tested with no measurable difference in the absorption component and, on close inspection (see inset Figure S11b), a slight

increase of t_{max} for the prominent nucleation component. This minor decrease in the nucleation kinetics indicates a slightly more compact nature as $t_{initial}$ increased.

Conclusions

The thermodynamics and kinetics of ion intercalation into a floating film of zinc porphyrin interfacial nanostructures (ZnPor-INs) were probed electrochemically without the need to support the ZnPor-IN film on a conductive electrode substrate. Instead, the film was supported on an electrified liquid|liquid interface and could be regarded to a mixed-solvent layer separating the aqueous and organic solutions. The electrochemical signal was due to purely ionic processes, not linked to redox reactions.

The film behaves as a capacitor. The ZnPor-IN film is electroneutral and the concentration of free ions is relatively small because of solvation effects. On increasing the negative polarisation of the interface, $\Delta_o^w\phi < 0$, the organic ammonium cations (R_2N^+) from the organic phase enter the film and intercalate the ZnPor-IN. Then, a few neutral carboxyl (–COOH) groups are forced to dissociate, and many more transform into $–COOR_2N$. In both cases, the released H^+ ions leave the film and enter the aqueous phase. The charge of the anionic carboxyl groups ($–COO^–$) is mostly compensated by free R_2N^+ ions. The total (*i.e.*, free and bound) R_2N^+ concentration in the film, $c_{COOR_2N} + c_{R_2N}^{IN}$, is a measure of the positive charge accumulated in the film as a capacitor; the negative charge in the capacitor corresponds to H^+ ions leaving the film (where there were bound as –COOH). To a lesser extent, aqueous citrate ($HCit^{2–}$) anions and lithium (Li^+) ions may also participate in this capacitive film behaviour.

The shape of the CV was distinctive, formed by the superposition of a narrow peak and a broad peak. The former indicated a positive cooperativity mechanism for ion intercalation and was attributed to structural rearrangements of the porphyrins at the electrified liquid|liquid interface during R_2N^+ intercalation. Employing the Frumkin isotherm, experimental CVs were simulated with negative g interaction parameters in line with those observed for a Li^+ intercalation process, a system with very similar underlying thermodynamics.[13] The kinetics of R_2N^+ intercalation were investigated by potential-step chronoamperometry. Depending on the applied interfacial Gavani potential $\Delta_o^w\phi$ and the interfacial concentration Γ_{ZnPor} of ZnPor, current transients presented a decay and multiple nucleation components. The latter was associated with domains where, due to structural rearrangements of the porphyrins, the electrochemically-driven binding and ion exchange of R_2N^+ took place faster. The nucleation

kinetics were seen to increase as the final potential $\Delta_o^w\phi_{final}$ was set to more negative values and decrease as Γ_{ZnPor} increased.

Overall, using electrified liquid|liquid interfaces, there is clearly significant potential to study, for the time, by electrochemical methodologies the dynamics of ion intercalation into solid matrices that are non-electronically conductive and/or that operate as non-electronically connected device components (for example ion exchange membranes). Such insights may critically influence the performance of a multitude of devices (Li-ion batteries, supercapacitors, fuel cells, electrolysers, *etc.*) with energy-related applications.

Supporting Information.

Complete experimental methods (Figures S1-S2); additional electrochemistry of the floating film of ZnPor-INs at the ITIES (Scheme 1, Figures S3-S7, Tables S1-S2); further details on modelling the electrochemistry of the floating film of ZnPor-INs at the ITIES (Figure S8, Tables S3-S5); further details on the kinetics of structural changes in the ZnPor-IN film during electrochemically-driven reversible ion intercalation (Figures S9-S11, Table S6).

Mathematica code for Figure 3 (PDF file).

Mathematica code for Figures 4 and S8 (PDF file).

Author Contributions

The manuscript was written through contributions of all authors.

Acknowledgements

M.D.S. acknowledges Science Foundation Ireland (SFI) under Grant no. 13/SIRG/2137 and the European Research Council through a Starting Grant (Agreement no. 716792). A. G.-Q. acknowledges funding received from an Irish Research Council Government of Ireland Postdoctoral Fellowship Award (grant number GOIPD/2018/252). J.A.M. acknowledges the Ministerio de Ciencia e Innovación (Spain) and the European Regional Development Funds (FEDER), project No. PGC2018-097359-B-I00.

Abbreviations

CV, cyclic voltammogram; IEM, ion exchange membrane; ITIES, interface between two immiscible electrolyte solutions; PPW, polarisable potential window; PZC, potential of zero charge; ZnPor-INs, zinc porphyrin interfacial nanostructures.

References

(1) Augustyn, V.; McDowell, M. T.; Vojvodic, A. Toward an Atomistic Understanding of Solid-State Electrochemical Interfaces for Energy Storage. *Joule* **2018**, *2* (11), 2189–2193. https://doi.org/10.1016/j.joule.2018.10.014.

(2) Stamenkovic, V. R.; Strmcnik, D.; Lopes, P. P.; Markovic, N. M. Energy and Fuels from Electrochemical Interfaces. *Nat. Mater.* **2016**, *16* (1), 57–69. https://doi.org/10.1038/nmat4738.

(3) Bazant, M. Z. Theory of Chemical Kinetics and Charge Transfer Based on Nonequilibrium Thermodynamics. *Acc. Chem. Res.* **2013**, *46* (5), 1144–1160. https://doi.org/10.1021/ar300145c.

(4) Kuznetsov, A. M.; Ulstrup, J. Theory of Electron Transfer at Electrified Interfaces. *Electrochim. Acta* **2000**, *45* (15–16), 2339–2361. https://doi.org/10.1016/S0013-4686(00)00336-4.

(5) Fong, K. D.; Wang, T.; Smoukov, S. K. Multidimensional Performance Optimization of Conducting Polymer-Based Supercapacitor Electrodes. *Sustain. Energy Fuels* **2017**, *1* (9), 1857–1874. https://doi.org/10.1039/c7se00339k.

(6) Strathmann, H. Electromembrane Processes: Basic Aspects and Applications. In *Comprehensive Membrane Science and Engineering*; Elsevier, 2010; Vol. 2, pp 391–429. https://doi.org/10.1016/B978-0-08-093250-7.00048-7.

(7) Strathmann, H.; Grabowski, A.; Eigenberger, G. Electromembrane Processes, Efficient and Versatile Tools in a Sustainable Industrial Development. *Desalination* **2006**, *199* (1–3), 1–3. https://doi.org/10.1016/j.desal.2006.03.130.

(8) Peighambardoust, S. J.; Rowshanzamir, S.; Amjadi, M. Review of the Proton Exchange Membranes for Fuel Cell Applications. *Int. J. Hydrogen Energy* **2010**, *35* (17), 9349–9384. https://doi.org/10.1016/j.ijhydene.2010.05.017.

(9) Yuzer, B.; Selcuk, H.; Chehade, G.; Demir, M. E.; Dincer, I. Evaluation of Hydrogen Production via Electrolysis with Ion Exchange Membranes. *Energy* **2020**, *190*, 116420. https://doi.org/10.1016/j.energy.2019.116420.

(10) Nguyen, T. D.; Whitehead, A.; Wai, N.; Ong, S. J. H.; Scherer, G. G.; Xu, Z. J. Equilibrium and Dynamic Absorption of Electrolyte Species in Cation/Anion Exchange Membranes of Vanadium Redox Flow Batteries. *ChemSusChem* **2019**, *12* (5), 1076–1083. https://doi.org/10.1002/cssc.201802522.

(11) Logan, B. E.; Elimelech, M. Membrane-Based Processes for Sustainable Power Generation Using Water. *Nature* **2012**, *488* (7411), 313–319. https://doi.org/10.1038/nature11477.

(12) Oliot, M.; Galier, S.; Roux de Balmann, H.; Bergel, A. Ion Transport in Microbial Fuel Cells: Key Roles, Theory and Critical Review. *Appl. Energy* **2016**, *183*, 1682–1704. https://doi.org/10.1016/j.apenergy.2016.09.043.

(13) Levi, M. D. Solid-State Electrochemical Kinetics of Li-Ion Intercalation into Li[Sub 1−x]CoO[Sub 2]: Simultaneous Application of Electroanalytical Techniques SSCV, PITT, and EIS. *J. Electrochem. Soc.* **1999**, *146* (4), 1279. https://doi.org/10.1149/1.1391759.

(14) Levi, M. D.; Aurbach, D. Frumkin Intercalation Isotherm - a Tool for the Description of Lithium Insertion into Host Materials: A Review. *Electrochim. Acta* **1999**, *45* (1), 167–185. https://doi.org/10.1016/S0013-4686(99)00202-9.

(15) Conway, B. E. Two-Dimensional and Quasi-Two-Dimensional Isotherms for Li Intercalation and Upd Processes at Surfaces. *Electrochim. Acta* **1993**, *38* (9), 1249–1258. https://doi.org/10.1016/0013-4686(93)80055-5.

(16) Levi, M. D.; Cohen, Y. S.; Gofer, Y.; Aurbach, D. Electrochemical Responses of Active Metal Insertion Electrodes and Electronically Conducting Polymers: Common Features and New Insights. *Electrochim. Acta* **2004**, *49* (22-23 SPEC. ISS.), 3701–3710. https://doi.org/10.1016/j.electacta.2004.01.075.

(17) Vorotyntsev, M. A.; Daikhin, L. I.; Levi, M. D. Isotherms of Electrochemical Doping and Cyclic Voltammograms of Electroactive Polymer Films. *J. Electroanal. Chem.* **1992**, *332* (1–2), 213–235. https://doi.org/10.1016/0022-0728(92)80352-5.

(18) Sirisaksoontorn, W.; Lerner, M. M. Preparation of a Homologous Series of Tetraalkylammonium Graphite Intercalation Compounds. *Inorg. Chem.* **2013**, *52* (12), 7139–7144. https://doi.org/10.1021/ic400733k.

(19) Fogg, A. M.; Dunn, J. S.; Shyu, S.-G.; Cary, D. R.; O'Hare, D. Selective Ion-Exchange Intercalation of Isomeric Dicarboxylate Anions into the Layered Double Hydroxide [LiAl2 (OH) 6] Cl⊙ H2O. *Chem. Mater.* **1998**, *10* (1), 351–355.

(20) Samec, Z. Electrochemistry at the Interface between Two Immiscible Electrolyte Solutions (IUPAC Technical Report). *Pure Appl. Chem.* **2004**, *76* (12), 2147–2180. https://doi.org/10.1351/pac200476122147.

(21) Peljo, P.; Girault, H. H. Liquid/Liquid Interfaces, Electrochemistry At. In *Encyclopedia of Analytical Chemistry*; John Wiley & Sons, Ltd: Chichester, UK, 2012. https://doi.org/10.1002/9780470027318.a5306.pub2.

(22) Suárez-Herrera, M. F.; Cazade, P.-A.; Thompson, D.; Scanlon, M. D. Monitoring Transient Changes in the Structure of Water at a Polarised Liquid-Liquid Interface Using Electrocapillary Curves. *Electrochem. commun.* **2019**, *109* (October), 106564. https://doi.org/10.1016/j.elecom.2019.106564.

(23) Suárez-Herrera, M. F.; Scanlon, M. D. On the Non-Ideal Behaviour of Polarised Liquid-Liquid Interfaces. *Electrochim. Acta* **2019**, *328*, 135110. https://doi.org/10.1016/j.electacta.2019.135110.

(24) Senthilkumar, S.; Dryfe, R. A. W.; Saraswathi, R. Size-Selective Voltammetry: Modification of the Interface between Two Immiscible Electrolyte Solutions by Zeolite Y. *Langmuir* **2007**, *23* (6), 3455–3461. https://doi.org/10.1021/la0626353.

(25) Dryfe, R. A. W.; Holmes, S. M. Zeolitic Rectification of Electrochemical Ion Transfer. *J. Electroanal. Chem.* **2000**, *483* (1), 144–149. https://doi.org/10.1016/S0022-0728(99)00506-9.

(26) Lillie, G. C.; Dryfe, R. a; Holmes, S. M. Zeolite-Membrane Modulation of Simple and Facilitated Ion Transfer. *Analyst* **2001**, *126* (11), 1857–1860. https://doi.org/10.1039/b105056g.

(27) Jiang, X.; Gao, K.; Hu, D.; Wang, H.; Bian, S.; Chen, Y. Ion-Transfer Voltammetric Determination of Folic Acid at Meso-Liquid-Liquid Interface Arrays. *Analyst* **2015**, *140* (8), 2823–2833. https://doi.org/10.1039/c4an02011a.

(28) Huang, X.; Xie, L.; Lin, X.; Su, B. Permselective Ion Transport Across the Nanoscopic Liquid/Liquid Interface Array. *Anal. Chem.* **2016**, *88* (12), 6563–6569. https://doi.org/10.1021/acs.analchem.6b01383.

(29) Xie, L.; Huang, X.; Lin, X.; Su, B. Nanoscopic Liquid/Liquid Interface Arrays Supported by Silica Isoporous Membranes: Trans-Membrane Resistance and Ion Transfer Reactions. *J. Electroanal. Chem.* **2017**, *784*, 62–68. https://doi.org/10.1016/j.jelechem.2016.12.007.

(30) Collins, M. C.; Hébrant, M.; Herzog, G. Ion Transfer at Polarised Liquid-Liquid Interfaces Modified with Adsorbed Silica Nanoparticles. *Electrochim. Acta* **2018**, *282*, 155–162. https://doi.org/10.1016/j.electacta.2018.06.036.

(31) Poltorak, L.; Gamero-Quijano, A.; Herzog, G.; Walcarius, A. Decorating Soft Electrified Interfaces: From Molecular Assemblies to Nano-Objects. *Appl. Mater. Today* **2017**, *9*, 533–550. https://doi.org/10.1016/j.apmt.2017.10.001.

(32) Stephenson, M. J.; Holmes, S. M.; Dryfe, R. A. W. Electrochemically Controlled Ion Exchange: Proton Exchange with Sodium Zeolite Y. *Angew. Chemie - Int. Ed.* **2005**, *44* (20), 3075–3078. https://doi.org/10.1002/anie.200463036.

(33) Stephenson, M. J.; Attfield, M. P.; Holmes, S. M.; Dryfe, R. A. W. Electrochemically Controlled Ion Exchange: Proton Ion Exchange with Sodium Zeolite X and A. *J. Solid State Electrochem.* **2015**, *19* (7), 1985–1992. https://doi.org/10.1007/s10008-015-2851-6.

(34) Stephenson, M. J.; Dryfe, R. A. W. Electrochemically Controlled Ion Exchange: Copper Ion Exchange with Sodium Zeolite Y. *Electrochim. Acta* **2007**, *53* (3 SPEC. ISS.), 1182–1188. https://doi.org/10.1016/j.electacta.2007.03.055.

(35) Otero, T. F.; Grande, H. J.; Rodríguez, J. Reinterpretation of Polypyrrole Electrochemistry after Consideration of Conformational Relaxation Processes. *J. Phys. Chem. B* **1997**, *101* (19), 3688–3697. https://doi.org/10.1021/jp9630277.

(36) Molina-Osorio, A. F.; Cheung, D.; O'Dwyer, C.; Stewart, A. A.; Dossot, M.; Herzog, G.; Scanlon, M. D. Self-Assembly of Porphyrin Nanostructures at the Interface between Two Immiscible Liquids. *J. Phys. Chem. C* **2020**, *124* (12), 6929–6937. https://doi.org/10.1021/acs.jpcc.0c00437.

(37) Monroe, C. W.; Urbakh, M.; Kornyshev, A. A. Understanding the Anatomy of Capacitance at Interfaces between Two Immiscible Electrolytic Solutions. *J. Electroanal. Chem.* **2005**, *582* (1–2), 28–40. https://doi.org/10.1016/j.jelechem.2005.04.031.

(38) Huber, T.; Pecina, O.; Schmickler, W. Influence of the Ions on the Capacity of Liquid | Liquid Interfaces. *J. Electroanal. Chem.* **1999**, *467* (1), 203–206. https://doi.org/10.1016/S0022-0728(98)00466-5.

(39) Torrie, G. M.; Valleau, J. P. Double Layer Structure at the Interface between Two Immiscible Electrolyte Solutions. *J. Electroanal. Chem.* **1986**, *206* (1–2), 69–79. https://doi.org/10.1016/0022-0728(86)90257-3.

(40) Yufei, C.; Cunnane, V. J.; Schiffrin, D. J.; Murtomäki, L.; Kontturi, K. Interfacial Capacitance and Ionic Association at Electrified Liquid/Liquid Interfaces. *J. Chem. Soc., Faraday Trans.* **1991**, *87* (1), 107–114. https://doi.org/10.1039/FT9918700107.

(41) Pereira, C. M.; Martins, A.; Rocha, M.; Silva, C. J.; Silva, F. Differential Capacitance of Liquid/Liquid Interfaces: Effect of Electrolytes Present in Each Phase. *J. Chem. Soc. Faraday Trans.* **1994**, *90* (1), 143–148. https://doi.org/10.1039/ft9949000143.

(42) Bates, R. G.; Pinching, G. D. Additions and Corrections-Resolution of the Dissociation Constants of Citric Acid at 0 to 50 Degrees and Determination of Certain Related Thermodynamic Functions. *J. Am. Chem. Soc.* **1949**, *71* (12), 4165–4165. https://doi.org/10.1021/ja01180a622.

(43) Hölzle, M. H.; Retter, U.; Kolb, D. M. The Kinetics of Structural Changes in Cu Adlayers on Au(111). *J. Electroanal. Chem.* **1994**, *371* (1–2), 101–109. https://doi.org/10.1016/0022-0728(93)03235-H.

(44) Otero, T. F.; Boyano, I. Potentiostatic Oxidation of Polyaniline under Conformational Relaxation Control: Experimental and Theoretical Study. *J. Phys. Chem. B* **2003**, *107* (18), 4269–4276. https://doi.org/10.1021/jp0225222.

(45) Otero, T. F.; Boyano, I. Comparative Study of Conducting Polymers by the ESCR Model. *J. Phys. Chem. B* **2003**, *107* (28), 6730–6738. https://doi.org/10.1021/jp027748j.

(46) Nateghi, M. R.; Savabieh, B. Study of Polyaniline Oxidation Kinetics and Conformational Relaxation in Aqueous Acidic Solutions. *Electrochim. Acta* **2014**, *121*, 128–135. https://doi.org/10.1016/j.electacta.2013.12.111.

Table of Contents artwork